Deterministic and stochastic analyses of fracture processes in a brittle microstructure system

Vikas Tomar, Min Zhou [*]

George W. Woodruff School of Mechanical Engineering, Georgia Institute of Technology, Atlanta, GA 30332-0405, United States

Abstract

Variations in constituent properties, phase morphology, and phase distribution cause deformation and failure at the microstructural level to be inherently stochastic. This paper focuses on the stochasticity of fracture processes that arises as a result of measurement uncertainties in the properties of the constituents in the heterogeneous microstructures of an Al_2O_3/TiB_2 ceramic composite system. Basic postulate here is that for a microstructure local material properties vary around their macroscopically measured value with the macroscopically measured value being the mean of the variation. A micromechanical cohesive finite element framework with explicit resolution of arbitrary fracture patterns and arbitrary microstructural morphologies is used in the analyses carried out in this paper. The randomness in the constituent properties at any given point in the microstructure is specified relative to the local mean values of the corresponding properties. A deterministic analysis and a stochastic analysis are carried out simultaneously. The combination of determinism and stochasticity is achieved by integrating a perturbation analysis of the influence of stochastic property variations around their mean values and a deterministic analysis for the microstructure with the mean values of the constituent properties. Calculations are carried out for actual and idealized microstructures of the Al_2O_3/TiB_2 material system. Calculations focus on analyzing the fracture response variation with varying levels of variation of material properties for a particular microstructural morphology as well as on analyzing the variations in fracture response with variations in microstructural morphology. It is observed that microstructural morphology is intricately linked to the variations in fracture response when material properties have stochastic origin. A microstructure less prone to fracture shows higher variations in fracture response when compared to the one which offers least resistance to the crack propagation. In addition, for a particular microstructural morphology, the levels of variations in the crack surface area generated and the variations in the energy release rate are of the same order as the levels of variations in constituent properties. The observations support the conclusion that a material designer needs to make conservative estimates for a material's performance if its microstructural construction imparts uncertainty to local material properties.
© 2005 Elsevier Ltd. All rights reserved.

---

[*] Corresponding author. Tel.: +1 404 894 3294; fax: +1 404 894 0186.
E-mail address: min.zhou@me.gatech.edu (M. Zhou).

1. Introduction

The stochasticity in material behavior arises out of several factors. Arbitrary microstructural phase morphologies and material heterogeneities are one source. The variations of local properties from specimen to specimen are another source. The determination of microscopic bulk and interfacial properties has been primarily on an ad hoc basis partly due to the difficulty in obtaining direct measurements. For heterogeneous microstructures, the task is more challenging since phases and inter-phase boundaries have very small size scales and complicated geometry. Both the spatial property heterogeneity and the uncertainty in specification of the material properties at each location motivate the development of material behavior characterizations that reflect the stochastic nature of deformation with respect to sampling and independent material property specification. The effect due to microstructure is intrinsically size-dependent, reflecting the spatial size scales of the heterogeneities. This effect is also sensitive to the morphology or spatial distribution of heterogeneities. At the mesoscopic and microscopic levels, failure analyses should account for the range of behavior associated with the material property fluctuations (cf. [1,2]). On the other hand, the effect of local property variations associated with multiple samples and measurement uncertainties depends on the probability density distribution. Proper account of this effect is more important for cases where parameters are calibrated using only a small number of data points. In line with this development, the statistical quantification of fracture behavior of a material should be based on a proper consideration of the correlation among three elements: probability distributions characterizing the distribution of flaws and material properties, fracture mechanics and material microstructure. Commonly used approaches for statistical characterization of fracture in brittle materials based on the Weibull's weakest link theory, cf., Weibull [3,4], are almost exclusively based on the first element. Progress has been made in incorporating the other two elements into Weibull's weakest link theory. For example, Batdorf [5] analyzed the statistical nature of fracture under multiaxial states of stress, accounting for the role of microstructure. Duxbury et al. [6] found that the statistical variation of fracture behavior and the size effect are significantly dependent on the nature of flaw distribution. Dai and Frantziskonis [7] studied the effect of material heterogeneity on energy dissipation and crack network formation. Zhou and Molinari [8] carried out 3-dimensional dynamic fracture simulations in ceramics with flaw distributions based on Weibull's statistics. However, until recently there was no general approach for the analysis of fracture with explicit account of microstructural morphology, random variation of material properties, and fracture processes.

The effect of spatial property heterogeneity have been analyzed within deterministic frameworks using randomly varying property fields (cf., e.g., [9–12]) and material property fields obeying specific statistical distribution functions (cf., e.g. [13,14]). In order to properly characterize the effects of microstructure and constituent property variations, a large number of simulations are needed if such deterministic frameworks are to be used. The alternative is to pursue combined deterministic and stochastic analyses so that characterizations of both the fracture process and the range of fracture outcome can be obtained. This research uses a methodology for combined deterministic and stochastic analyses of dynamic fracture. The method is based on an integration of the cohesive finite element method (CFEM) and a second-order perturbation analysis. The CFEM framework used is that of Tomar et al. [15] and Zhai et al. [16]. The second-order perturbation analysis is that of Liu et al. [17] and has been applied in a variety of settings including foundations with random variations of soil properties (cf. [18]), plates and beams with random loads and random properties (cf. [19,20]), structures with non-linear responses (cf. [21,22]), and cracked specimens with stochastic J-integral and fracture toughness values (cf. [23,24]). With this framework, it is possible to obtain from one single calculation both a deterministic quantification of a fracture process and an estimate of the range of possible fracture outcome in terms of quantities such as stress distribution, strain field, crack length, crack speed, and energy release rate. This method is used here to characterize the effect of the random variations in material properties on the dynamic fracture behavior of an Al_2O_3/TiB_2 ceramic composite system, cf. Logan [25]. Hypothetical phase morphologies as well as

real phase arrangements with randomly varying constituent and interfacial properties are analyzed. In the following sections, the framework for combined deterministic and stochastic analyses is first described, followed by discussions on the results of calculations on the material behavior.

2. Formulation

Our approach for combined deterministic and stochastic analyses with explicit account of microstructure and fracture processes integrates the micromechanical cohesive finite element method (CFEM), cf. Zhai et al. [16], and a second-order perturbation analysis for linear finite element problems, cf. Liu et al. [17]. This integration involves the superposition of the perturbation analysis on top of the CFEM deterministic analysis of fracture. Specifically, the deterministic analysis is carried out for the material whose properties at each point are equal to the expectation values of the corresponding material parameters. The perturbation analysis is relative to the deterministic state at each time, with respect to the variations in material parameters. While the deterministic process follows the standard field equations of balance of momentum, kinematic, and constitutive equations, the perturbation analysis yields a sequential system of differential equations for the successive derivatives up to the second-order of the displacement. The successive derivatives of the displacement field are then used to characterize the stochastic outcome of material behavior. This characterization is in terms of the expectation value and the variance of quantities quantifying the deformation and failure of the microstructures analyzed (e.g., stress, crack length, and energy dissipated). While the deterministic analysis explicitly tracks fracture processes, the perturbation analysis focuses on the mean and standard deviations of independent variables (material properties) and dependent variables. The analysis is valid only for conditions under which variations in independent variables have narrow band characteristics and fluctuations of small magnitudes. Therefore, perturbation analyses up to the second-order can be carried out (cf. [26]) and only variations of up to 15% relative to mean values can be considered. This framework for finite element analyses is briefly outlined next.

2.1. Perturbation analysis

Variations in both bulk properties (Young's modulus E and Poisson's ratio v) and interfacial properties (interfacial strength $T_{\max}$ and critical separation Δ_{nc}) as discussed later are considered. In the discussion here, these quantities are collectively denoted by the random independent field vector $\mathbf{a}(\mathbf{x}) = (E, v, T_{\max}, \Delta_{nc}) = (a_1, a_2, a_3, a_4) = (a_j)$, $(j = 1, \ldots, p)$. In general, $a_j(\mathbf{x})$ can be any random material property field in the bulk and interfacial constitutive relations used and p is the total number of such independent fields. In this paper, $p = 4$. We denote $a_{ji} = a_j(\mathbf{x}_i)$ as the value at position $\mathbf{x}_i$ of the jth component in $\mathbf{a}$ (i.e., a_j). a_j is approximated through finite element shape functions $N_i(\mathbf{x})$ as

$$a_j(\mathbf{x}) = \sum_{i=1}^{q} N_i(\mathbf{x}) a_{j_i}. \tag{1}$$

Here, q is the number of interpolation points where a_j is specified. These points define a grid for property interpolation which coexists with the finite element mesh for the deformation analysis described in Section 2.2. In general, the triangulations and shape functions for the property interpolation and those for the deformation analysis are not the same. The interpolation grid associated Eq. (1) is usually coarser than the mesh for the deformation analysis. The size scale of the interpolation grid and the number of interpolation points (q) are closely related to the correlation length in the random fields. To carry out the perturbation analysis, we follow the notations of Liu et al. [17]. For $\mathbf{a}(\mathbf{x})$ and a given function $f[\mathbf{a}(\mathbf{x})]$, the following operations are defined.

$\bar{a}_j(\mathbf{x}) = \Xi[a_j(\mathbf{x})]$ mean or expectation value of $a_j(\mathbf{x})$

$a_{jr} = a_j(\mathbf{x}_r)$ value of $a_j(\mathbf{x})$ at an arbitrary position $\mathbf{x}_r$

$\mathrm{d}a_{jr} = \varepsilon\Delta a_{jr} = \varepsilon(a_{jr} - \bar{a}_{jr})$ first-order variation of a_{jr} about $\bar{a}_{jr}$

$\mathrm{d}a_{jr}\mathrm{d}a_{js} = \varepsilon^2\Delta a_{jr}\Delta a_{js}$ second-order variation of a_{jr} and a_{js} about $(\bar{a}_{jr}, \bar{a}_{js})$

$\bar{f}(\mathbf{x}) = f[\mathbf{x}, \bar{\mathbf{a}}(\mathbf{x})]$ value of f evaluated at $\bar{a}$, this value is not necessarily equal to the expectation value of f

$\bar{f}_{a_{jr}} = \frac{\partial f}{\partial a_{jr}}$ derivative of f with respect to a_{jr} evaluated at $\bar{a}_{jr}$; and

$\bar{f}_{a_{jr}a_{js}} = \frac{\partial^2 f}{\partial a_{jr}\partial a_{js}}$ mixed derivative of f w.r.t. a_{jr} and a_{js} evaluated at $(\bar{a}_{jr}, \bar{a}_{js})$.

In the above expressions, $\varepsilon \ll 1$ is a small parameter. Under Eq. (1), $a_j(\mathbf{x})$ is fully specified by the expectation values $\bar{a}_{ji}$ of nodal values a_{ji}, the coefficients of variation β_{ji} of a_{ji}, and the coefficients of correlation $R(a_{ji_1}, a_{ji_2})$ between a_{ji_1} and a_{ji_2}. Here, $i_1 = 1, \ldots, q$ and $i_2 = 1, \ldots, q$ are two different instances of $i = 1, \ldots, q$. Also, the mean and the variance of $a_j(x)$ are approximated through the shape functions as

$$\Xi[a_j(\mathbf{x})] = \sum_{i=1}^{q} N_i(\mathbf{x})\Xi(a_{ji}) \tag{2}$$

and

$$\mathrm{Var}[a_j(\mathbf{x})] = \sum_{i_1,i_2=1}^{q} N_{i_1}(\mathbf{x})N_{i_2}(\mathbf{x})\mathrm{Cov}(a_{ji_1}, a_{ji_2}). \tag{3}$$

In the above expression, $\mathrm{Cov}(a_{ji_1}, a_{ji_2})$ is the covariance between a_{ji_1} and a_{ji_2} in the form of

$$\mathrm{Cov}(a_{ji_1}, a_{ji_2}) = \sqrt{\mathrm{Var}(a_{ji_1})\mathrm{Var}(a_{ji_2})}R(a_{ji_1}, a_{ji_2}) \tag{4}$$

with

$$\mathrm{Var}(a_{ji}) = \beta_{ji}^2\Xi(a_{ji})^2. \tag{5}$$

The formulation here holds in general for material property fields that have spatially inhomogeneous random variation characteristics. In this paper, the random variation characteristics of the material property fields are assumed to be homogeneous. Accordingly, the coefficients of variation β_{ji} and the coefficients of correlation $R(a_{ji_1}, a_{ji_2})$ are spatially uniform. In particular, $R(a_{ji_1}, a_{ji_2})$ is assumed to be

$$R(a_{ji_1}, a_{ji_2}) = \exp\left[-(x_{i_1} - x_{i_2})^2/d_x^2\right]\exp\left[-(y_{i_1} - y_{i_2})^2/d_y^2\right], \tag{6}$$

where d_x and d_y are correlation length scales which specify the rate of decay of the spatial correlation in a random field. The perturbation analysis involves expressing a random dependent field $\mathbb{C}(\mathbf{x})$ (which can be, e.g., displacement, a stress component, a strain component, dissipated energy, a cohesive surface traction component, or a component of the cohesive surface separation) in terms of the expected values and variations of the independent field vectors $a_j = (a_{j1}, a_{j2}, \cdots, a_{jq})^{\mathrm{T}}$ as

$$\mathbb{C}(\mathbf{x}) = \overline{\mathbb{C}}(\mathbf{x}) + \sum_{j=1}^{p}\left[\sum_{i_1=1}^{q}(\overline{\mathbb{C}})_{a_{ji_1}}\Delta a_{ji} + \frac{1}{2}\sum_{i_1,i_2=1}^{q}(\overline{\mathbb{C}})_{a_{ji_1}a_{ji_2}}\Delta a_{ji_1}\Delta a_{ji_2}\right]. \tag{7}$$

The expected value of $\mathbb{C}$ is

$$\Xi(\mathbb{C}) = \int_{-\infty}^{\infty}\mathbb{C}(\mathbf{a})p(\mathbf{a})\mathrm{d}\mathbf{a} \tag{8}$$

with $p(\mathbf{a})$ being the joint probability density function for $\mathbf{a}$. A second-order estimate of $\Xi(\mathbb{C})$ obtained by inserting Eq. (7) into Eq. (8) is

$$\varXi(\mathbb{C}) = \overline{\mathbb{C}} + \frac{1}{2} \sum_{j=1}^{p} \left[\sum_{i_1,i_2=1}^{q} (\overline{\mathbb{C}})_{a_{ji_1} a_{ji_2}} \mathrm{Cov}(a_{ji_1}, a_{ji_2}) \right], \tag{9}$$

where $\overline{\mathbb{C}}$ is the value of $\mathbb{C}$ at $\bar{a}_j = (\bar{a}_{j1}, \bar{a}_{j2}, \ldots, \bar{a}_{jq})^{\mathrm{T}}$ and is not equal to the expectation value $\varXi(\mathbb{C})$ in general. The expression for the auto-covariance matrix of $\mathbb{C}$ is (cf. [17])

$$\mathrm{Cov}(\mathbb{C}_r, \mathbb{C}_s) = \varXi\big[(\mathbb{C}_r - \bar{\mathbb{C}}_r)(\mathbb{C}_s - \bar{\mathbb{C}}_s)\big] = \int_{-\infty}^{\infty} (\mathbb{C}_r - \bar{\mathbb{C}}_r)(\mathbb{C}_s - \bar{\mathbb{C}}_s) p(\mathbf{a}) \mathrm{d}\mathbf{a}, \tag{10}$$

where $\mathbb{C}_r = (\mathbf{x}_r)$. The corresponding first-order-accurate covariance $\mathrm{Cov}(\mathbb{C}_r, \mathbb{C}_s)$ consistent with the second-order perturbation analysis is

$$\mathrm{Cov}(\mathbb{C}_r, \mathbb{C}_s) = \sum_{j=1}^{p} \sum_{i_1,i_2=1}^{q} (\overline{\mathbb{C}}_r)_{a_{ji_1}} (\overline{\mathbb{C}}_s)_{a_{ji_2}} \mathrm{Cov}(a_{ji_1}, a_{ji_2}). \tag{11}$$

In the analysis here, only the expected value and the variance of $\mathbb{C}$ are of interest. Also, the random material property fields have been assumed to be independent of each other, leading to $\mathrm{Cov}(a_{j_1 i_1}, a_{j_2 i_2}) = 0$ if $j_1 \neq j_2$.

For material property variations within 15% of respective mean values, the second-order perturbation analysis has been shown to give results consistent with those of the direct Monte Carlo method (c.f. [23,26]). Analyses typically involve property variations of the order of 15% random with narrow band characteristics. The advantage of this method is that the multivariate distribution function for input parameters need not be known.

2.2. Finite element framework

A Lagrangian finite deformation formulation is used to account for the finite strains and rotations in crack tip regions. For details reader is referred to Tomar et al. [15] and Zhai et al. [16]. The volumetric constitutive law is hyperelastic so that

$$\sigma = \frac{\partial W}{\partial \mathbf{E}}, \tag{12}$$

where, $\sigma = \mathbf{s} \cdot \mathbf{F}^{-\mathrm{T}}$ is the second Piola–Kirchoff stress tensor. W is the strain energy density, taken to be,

$$W = \frac{1}{2} \mathbf{E} : \mathbf{L} : \mathbf{E} \tag{13}$$

with

$$\mathbf{L} = \frac{E}{1+v} \left(\mathbf{II} + \frac{v}{1-2v} \mathbf{I} \otimes \mathbf{I} \right) \tag{14}$$

being the tensor of isotropic elastic moduli. E and v are the Young's modulus and Poisson's ratio, respectively. $\mathbf{E}$ is the Lagrangian strain given by,

$$\mathbf{E} = \frac{1}{2} \big(\mathbf{F}^{\mathrm{T}} \cdot \mathbf{F} - \mathbf{I} \big). \tag{15}$$

In the above formulae, $\mathbf{II}$ is the fourth-order identity tensor, $\mathbf{F}$ is deformation gradient tensor, $\mathbf{I}$ is the second-order identity tensor, $\mathbf{I} \otimes \mathbf{I}$ denotes the outer product of two second-order tensors, and $()^{\mathrm{T}}$ and $()^{-\mathrm{T}}$ denote transpose and inverse transpose, respectively. A review of various types of cohesive laws is given by Shet and Chandra [27]. In this research we use a variable stiffness bilinear cohesive traction-separation relation, cf. Tomar et al. [15]. The finite element discretization leads to a system of linear algebraic equations of the form

$$\mathbf{M}\frac{\partial^2 \mathbf{U}}{\partial t^2} = -\mathbf{R}, \tag{16}$$

where, $\mathbf{U}$ is the vector of nodal displacements, $\mathbf{M}$ is the nodal mass matrix and $\mathbf{R}$ is the nodal force vector consisting of contributions from both the bulk elements and the cohesive surfaces, i.e. $\mathbf{R} = \mathbf{R}^b + \mathbf{R}^c$, where $\mathbf{R}^b = \int_V \mathbf{B}^{\mathrm{T}} s \mathrm{d}V$ and $\mathbf{R}^c = \int_{S_{\mathrm{int}}} \mathbf{N}^{\mathrm{T}} \mathbf{T} \mathrm{d}S$ denote the force vector contributions from bulk elements and cohesive surfaces, respectively. Here, N denotes the finite element shape function and $\mathbf{B}$ is the spatial gradient of $\mathbf{N}$. Krieg and Key [28] showed that from the point of view of accuracy as well as computational efficiency lumped mass matrix is preferable for explicit time integration procedures. Therefore, a lumped mass matrix $\mathbf{M}$ is used in Eq. (16) instead of the consistent mass matrix. The explicit time-integration scheme based on the Newmark β-method with $\beta = 0$ and $\gamma = 0.5$ is employed to integrate Eq. (16), c.f. Belytschko et al. [29]. The displacements and velocities at $t_{n+1} = t_n + \Delta t_n$ are obtained by integrating the equations of motion using Newmark β-method as

$$\left.\begin{array}{l} \ddot{\mathbf{U}}^{n+1} = \mathbf{M}^{-1}\mathbf{R} \\[2mm] \dot{\mathbf{U}}^{n+1} = \dot{\mathbf{U}}^n + \frac{1}{2}\Delta t_{\mathrm{n}}\left(\ddot{\mathbf{U}}^{n+1} + \ddot{\mathbf{U}}^n\right) \quad \text{and} \\[2mm] \mathbf{U}^{n+1} = \mathbf{U}^n + \Delta t_{\mathrm{n}}\dot{\mathbf{U}}^n + \frac{1}{2}(\Delta t_{\mathrm{n}})^2\ddot{\mathbf{U}}^n \end{array}\right\}. \tag{17}$$

Here, $(\cdot)^{-1}$ denotes the matrix inverse, $\ddot{\mathbf{U}} = \partial^2 \mathbf{U}/\partial t^2$ and $\dot{\mathbf{U}} = \partial \mathbf{U}/\partial t$. In Eq. (16), the mass matrix $\mathbf{M}$ is deterministic while the acceleration vector and the force vector are random functions in the forms of $\ddot{\mathbf{U}}(\mathbf{x}, \mathbf{a})$ and $\mathbf{R}(\mathbf{x}, \mathbf{a})$, respectively. The basic idea in the analysis is to expand $\ddot{\mathbf{U}}$ and $\mathbf{R}$ about $\bar{a}$ of $\mathbf{a}(\mathbf{x})$ and to retain terms of up to second-order. The systems of differential algebraic equations for the zeroth, first and second-order moments of $\ddot{\mathbf{U}}$ in terms of the zeroth, first and second-order moments of R, respectively, are obtained. These moments are then used to calculate the mean value and the variance of $\ddot{\mathbf{U}}$ in terms of the independent properties. Similarly, the stochastic moments, the expected value and the variance for elemental stresses, elemental strains, bulk tractions, cohesive traction, cohesive separation and global force vector are obtained, cf. Tomar and Zhou [30].

2.3. Cohesive relation

The bilinear cohesive relation used here contains an independent variable to admit finite initial stiffness of the cohesive surfaces, cf. Tomar et al. [15] and Zhai et al. [16]. For simplicity, only tensile loading is considered. An extension to account for compressive loading is discussed in Minnaar [31]. This relation is derived from a potential Φ which is a function of separation Δ through a state variable defined as $\lambda = \sqrt{(\Delta_{\mathrm{n}}/\Delta_{\mathrm{nc}})^2 + (\Delta_{\mathrm{t}}/\Delta_{\mathrm{tc}})^2}$. This variable describes the effective instantaneous state of mixed-mode separations. Here, $\Delta_n = \mathbf{n} \cdot \mathbf{\Delta}$ and $\Delta_t = \mathbf{t} \cdot \mathbf{\Delta}$ denote, respectively, the normal and tangential components of Δ, with $\mathbf{n}$ and $\mathbf{t}$ being unit vectors normal and tangent to S_0 respectively. Δ_{nc} is the critical normal separation at which the cohesive strength of an interface vanishes under conditions of pure normal deformation ($\Delta_t = 0$). Similarly, Δ_{tc} is the critical tangential separation at which the cohesive strength of an interface vanishes under conditions of pure shear deformation ($\Delta_n = 0$). λ tracks instantaneous mixed-mode separations during both loading and unloading. Clearly, $\lambda = 0$ corresponds to $\mathbf{\Delta} = 0$ (undeformed state or fully unloaded state) and $\lambda \geqslant 1$ implies complete separation, i.e. total debonding of the cohesive surface pair. In order to account for the irreversibility of separations, a parameter $\eta = \max\{\eta_0, \lambda_{\mathrm{ul}}\}$ is defined. As illustrated in Fig. 1(a), η_0 is the initial value of η which defines the stiffness of the original undamaged cohesive surface and λ_{ul} is the hitherto maximum value of λ at which an unloading process was initiated. Note that λ_{ul} is associated with the onset of an unloading event and is not necessarily the hitherto maximum value of λ.
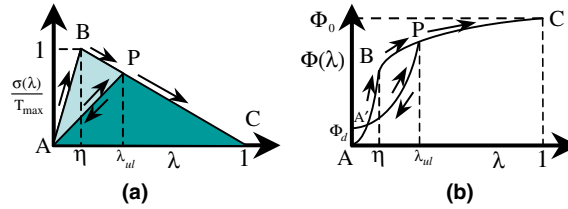
Fig. 1. Irreversible cohesive relation.

Obviously, λ_{ul} represents the (reduced) current stiffness of the cohesive surfaces after damage and unloading have occurred. Also, one always has $\eta < 1$. While η_0 is the characteristic value of effective separation λ at which the effective traction σ (see below) for a cohesive surface pair reaches the strength T_{max} of the undamaged surface, λ_{ul} is the critical level of λ at which σ reaches the reduced strength $T_{max}(1 - \eta)/(1 - \eta_0)$ of the hitherto damaged cohesive surface pair. The specific form for the potential is taken as

$$\Phi = \Phi(\lambda, \eta) = \begin{cases} \Phi_0 \left(\dfrac{1 - \eta}{1 - \eta_0} \right) \left(\dfrac{\lambda^2}{\eta} \right), & \text{if } 0 \leqslant \lambda \leqslant \eta, \\[3mm] \Phi_0 \left(\dfrac{1 - \eta}{1 - \eta_0} \right) \left(1 - \dfrac{(1 - \lambda)^2}{1 - \eta} \right), & \text{if } \eta < \lambda \leqslant 1. \end{cases} \tag{18}$$

This relation allows the traction to be defined through

$$\mathbf{T} = \frac{\partial \Phi}{\partial \mathbf{\Delta}} \tag{19}$$

yielding the normal and shear traction components as

$$T_n = \sigma(\lambda, \eta) \frac{\Delta_n}{\lambda \Delta_{nc}} \quad \text{and} \quad T_t = \sigma(\lambda, \eta) \frac{\alpha \Delta_t}{\lambda \Delta_{tc}}. \tag{20}$$

In the above expressions, $\alpha = \Delta_{nc}/\Delta_{tc}$ and

$$\sigma = \sqrt{(T_n)^2 + (T_t/\alpha)^2} = \begin{cases} \left(T_{max} \dfrac{1 - \eta}{1 - \eta_0} \right) \dfrac{\lambda}{\eta}, & \text{if } 0 \leqslant \lambda \leqslant \eta, \\[3mm] \left(T_{max} \dfrac{1 - \eta}{1 - \eta_0} \right) \dfrac{1 - \lambda}{1 - \eta}, & \text{if } \eta < \lambda \leqslant 1, \\[3mm] 0, & \text{if } \lambda > 1. \end{cases} \tag{21}$$

For a surface that has previously been deformed to $\lambda = \eta$ and has experienced unloading from this value of λ, the work of separation for an arbitrary separation process is (see Eqs. (18) and (19))

$$\int_0^{\Delta_c} \mathbf{T} \cdot \mathrm{d}\Delta = \Phi(1, \eta), \tag{22}$$

where Δ_c is the critical separation under general mixed mode conditions at which σ vanishes and by definition $\lambda(\Delta_c) = 1$. In particular, for pure normal separations $\Delta_c = \{\Delta_{nc}, 0\}$ and for pure tangential separations $\Delta_c = \{0, \Delta_{tc}\}$. Since the unloading and reloading along AP (Fig. 1(a)) are fully elastic, the amount of work required to fully separate a unit surface area from the undamaged state is

$$\int_0^{\Delta_c} \mathbf{T} \cdot \mathrm{d}\Delta = \Phi(1, \eta_0) = \Phi_0. \tag{23}$$

This constant can be calibrated through pure normal and pure shear separations, i.e.

$$
\begin{aligned}
\Phi_0 &= \int_0^{\Delta_{nc}} T_n \mathrm{d}\Delta_n = \int_0^{\eta_0 \Delta_{nc}} \left(T_{max} \frac{\Delta_n}{\eta_0 \Delta_{nc}} \right) \mathrm{d}\Delta_n + \int_{\eta_0 \Delta_{nc}}^{\Delta_{nc}} \left(T_{max} \frac{1 - \dfrac{\Delta_n}{\Delta_{nc}}}{1 - \eta_0} \right) \mathrm{d}\Delta_n \\
&= \int_0^{\Delta_{tc}} T_t \mathrm{d}\Delta_t = \int_0^{\eta_0 \Delta_{tc}} \left(T_{max} \frac{\alpha \Delta_t}{\eta_0 \Delta_{tc}} \right) \mathrm{d}\Delta_t + \int_{\eta_0 \Delta_{tc}}^{\Delta_{tc}} \left(\alpha T_{max} \frac{1 - \dfrac{\Delta_t}{\Delta_{tc}}}{1 - \eta_0} \right) \mathrm{d}\Delta_t \\
&= \frac{1}{2} T_n^{max} \Delta_{nc} = \frac{1}{2} \alpha T_n^{max} \Delta_{tc}.
\end{aligned}
\tag{24}
$$

Apparently, $T_{max} = T_n^{max}$ is the maximum cohesive traction under conditions of pure normal separation. While the bilinear relationship between σ and λ embodied in the above formulation is illustrated in Fig. 1(a), the variation of Φ is shown in Fig. 1(b). Overall, five parameters are needed to specify the cohesive behavior, including the maximum tensile strength T_{max}, the critical separations Δ_{nc} and Δ_{tc}, characteristic separation η_0, and α. It is clear that for fixed values of characteristic separation η_0, and α, the maximum tensile strength T_{max}, the critical separations Δ_{nc} can be taken as the independent parameters of the cohesive law. Correspondingly, the stochastic moments for cohesive traction vector **T** and separation variable λ are calculated based on the random fields of T_{max} and Δ_{nc}.

Eq. (21) describes a two-stage behavior as illustrated in Fig. 1. Between A and B ($0 \leqslant \lambda \leqslant \eta_0$), separation occurs elastically and the cohesive energy stored (work done in causing separation) is fully recoverable. Damage in the form of microcracks and other small-scale defects does not occur. Between B and C ($\eta_0 \leqslant \lambda \leqslant 1$), material degradation causes progressive reduction in the strength of the cohesive surfaces. This represents a phenomenological account of the effects of microcracks and other defects not explicitly modeled in the CFEM framework. Unloading from any point P follows path PA and subsequent reloading follows AP and then PC. Part of the work expended on causing the separation in this regime is irrecoverable, as indicated by the hysteresis loop ABP which implies dissipation during the softening process. Correspondingly, there is a decrease in the maximum tensile strength of the cohesive surface. This is reflected in the elastic reloading of the interface along AP and further softening along path PC. To correctly account for this behavior, it is necessary to record the value of λ_{ul}. We must point out that the dependence of the damaged behavior on previous deformation is very week and limited, only through η which tracks the hitherto largest extend of separation from which unloading has occurred. Any other aspect of preceding loading–unloading cycles does not in any way influence the deformation. This behavior is similar to the Markov chain (c.f., e.g., Lin [32]) in stochastic analyses. Since any unloading and reloading (along PA in Fig. 1(a) or PA′ in Fig. 1(b)) are elastic, the amount of work that has been dissipated is

$$
\Phi_d(\lambda, \eta) = \begin{cases}
0, & \text{if } \lambda \leqslant \eta_0, \\
\Phi(\eta, \eta_0) - \Phi(\eta, \eta) = \dfrac{\eta - \eta_0}{1 - \eta_0} \Phi_0, & \text{if } \eta_0 < \lambda \leqslant \eta, \\
\Phi(\lambda, \eta_0) - \Phi(\lambda, \eta) = \dfrac{\lambda - \eta_0}{1 - \eta_0} \Phi_0, & \text{if } \eta < \lambda \leqslant 1, \\
\Phi_0 & \text{if } \lambda > 1.
\end{cases}
\tag{25}
$$

Note here that $\eta_0 < \eta = \max\{\eta_0, \lambda_{ul}\} < 1$ and that η never attains the value of 1. The dissipation is uniquely defined and $\Phi_d(\lambda, \eta)$ is a monotonically increasing function. When full separation is achieved, $\Phi_d(1, \eta) = \Phi_0$. Φ_d is partly converted into the surface energy and partly spent on causing damage in the material adjacent

to crack surfaces through microcrack formation not explicitly modeled. A unique damage parameter can be defined to phenomenologically track the progressive softening of cohesive surfaces interspersed throughout the composite microstructure. This parameter D is defined such that

$$D = \frac{\Phi_d}{\Phi_0}, \tag{26}$$

$0 \leqslant D \leqslant 1$, with $D = 0$ indicating fully recoverable interfacial separation and $D = 1$ signifying complete separation or total fracture. In the numerical analysis carried out in Zhai et al. [16] and in this paper, D is used as a state variable quantifying the degree of the damage, providing a phenomenological measure for failure analysis. The spatial and time variation of $D = D(\mathbf{x}, t)$ allows the distribution and evolution of damage in various microstructures to be analyzed.

The probability corresponding to a confidence interval of a random variable can be estimated using the Chebyshev inequality which is reduced from a more general expression for the time envelope of a random process (c.f. Nigam [33]). The Chebyshev inequality

$$P(|(X - \mu)| \geqslant n s_d) \leqslant 1/n^2 \tag{27}$$

provides a conservative estimate for the probability in terms of the mean and variance of random variable X without any stipulation about the nature of its probability distribution. Here, $P(\cdot)$ stands for probability and n is an integer. The probability of X being outside the interval of $\mu \pm 3 s_d$ is less than or equal to 0.11 and the probability for being outside the interval of $\mu \pm 6 s_d$ is less than or equal to 0.027. To state differently, the probability for X to fall within the interval $\mu \pm 3 s_d$ is at least 0.89 and the probability for it to fall within the interval $\mu \pm 6 s_d$ is at least 99.973. Since the crack length, crack initiation time, and damage parameter depend on λ, their stochastic variations depend on the variation of λ. To characterize this dependence, the expected value μ^λ and the standard deviation s_d^λ of λ are obtained based on the analysis in Section 2.1. In this characterization, the range of variation of λ is taken as $\mu^\lambda \pm 6 s_d^\lambda$ which corresponds to a cumulative probability of at least 99.973%.

The finite element mesh used consists of "cross-triangle" elements of equal dimensions arranged in a quadrilateral pattern. Cohesive surfaces are embedded along all finite element boundaries as part of the physical model. The model parameters are the same those in Zhai et al. [16] and are shown in Table 1.

It is important to note that since the stochastic variations of $T_{\max}$ and Δ_{nc} are independent of each other, the cohesive energy Φ_0 also varies stochastically. This is a more general and more realistic characterization. It is different from other analyses (e.g., that of Xuan et al. [12]) in which Φ_0 is maintained constant while parameters such as $T_{\max}$ and Δ_{nc} are varied accordingly. The range of the density of energy dissipated Φ_d is defined as $\mu^{\Phi_d} \pm 6 s_d^{\Phi_d}$ with a confidence level of at least 99.973%. The corresponding lower limit, expected value, and upper limit for this range are $\Phi_d^{low} = \mu^{\Phi_d} - 6 s_d^{\Phi_d}$, $\Phi_d^{expect} = \mu^{\Phi_d}$, and $\Phi_d^{upper} = \mu^{\Phi_d} + 6 s_d^{\Phi_d}$, respectively. Here, μ^{Φ_d} stands for the mean value of Φ_d. Under this condition, the range of the total energy dissipated $\phi = \int_{S_0} \Phi_d \, dS$ is taken as $\mu^\phi \pm 6 s_d^\phi$ ($\phi_d^{low} = \mu^\phi - 6 s_d^\phi$, $\phi_d^{expect} = \mu^\phi$ and $\phi_d^{upper} = \mu^\phi + 6 s_d^\phi$). The standard deviation $s_d^{\phi_0}$ of ϕ is obtained by taking the square root of the variance of ϕ. The mean value and the variance of Φ_d are calculated from its stochastic moments. The energy release rate G here is calculated by dividing the total energy dissipated by the total crack surface generated. This is a phenomenological

Table 1
Bulk and interfacial parameters

Compound	Density (kg/m³)	K_{IC} MPa $\sqrt{m}$	E (GPa)	v	$T_{\max}$ (GPa)	Δ_{nc}, Δ_{tc} (nm)	Φ_0 (J/m²)
Al₂O₃	3990	4.0	340	0.23	0.5	100	25
TiB₂	4520	7.2	500	0.12	1.0	100	50
Homogenized Al₂O₃/TiB₂ composite	4120	3.6	415	0.15	0.65	100	32.5
Al₂O₃/TiB₂ interface	–	–	–	–	0.5	100	25

parameter that accounts for multiple crack tips and non-self similar crack growth. For 2D calculations, the range of this average energy release rate is characterized by $\overline{G}_{\text{low}} = \phi_{\text{d}}^{\text{low}}/l^{\text{low}}$, $\overline{G}_{\text{exp}} = \phi_{\text{d}}^{\text{expect}}/l^{\text{expect}}$, and $\overline{G}_{\text{high}} = \phi_{\text{d}}^{\text{upper}}/l^{\text{upper}}$. Here, l^{low}, l^{exp}, and l^{high} denote the lower limit, mean, and upper limit of crack length l, respectively.

3. Calculations and results

Computations are carried out for a center-cracked Al_2O_3/TiB_2 specimen under tensile loading. The specimen configuration is shown in Fig. 2. One half of the specimen is used in the calculations due to symmetry. The whole specimen has a width of $2W = 2$ mm and a height of $2H = 0.6$ mm. The length of the initial crack is $2a_i = 0.4$ mm. The specimen is stress free and at rest initially. Tensile loading is applied by imposing symmetric velocity boundary conditions along the upper and the lower edges of the specimen. Conditions of plain strain are assumed to prevail. The finite element mesh used is shown in Fig. 3. Finer elements are used in the small region in front of the crack tip in order to resolve the high stress gradients and the microstructures analyzed. The mesh consists of "cross-triangle" elements arranged in a quadrilateral pattern. The size of the quadrilaterals next to the crack tip is 2 µm. This element size is within the upper and lower bounds required for solution convergence for CFEM models with cohesive surfaces along all element boundaries, as discussed in Tomar et al. [15]. An analysis of the effect of microstructural window size on model predictions has also been carried out in Tomar et al. [15]. The dimensions of 40×500 µm for the real micrographs and 60×300 µm for the hypothetical phase arrangements are found to be suitable for the microstructural window. These window sizes are much larger than the length scales involved in both types of microstructures, allowing sufficient representations of the microstructures. The analyses carried out here are limited only to lengths of crack propagation within the microstructural regions. Therefore, stochastic perturbations are introduced only in the microstructural window. Material outside this window is assumed to be homogeneous and is assigned effective properties representative of those for the Al_2O_3/TiB_2 ceramic composite (see Table 1). Both regions are discretized in the same manner, involving both bulk element and cohesive surface elements. For the results discussed here, the imposed boundary velocity of $V_0 = 2$ m/s is applied on
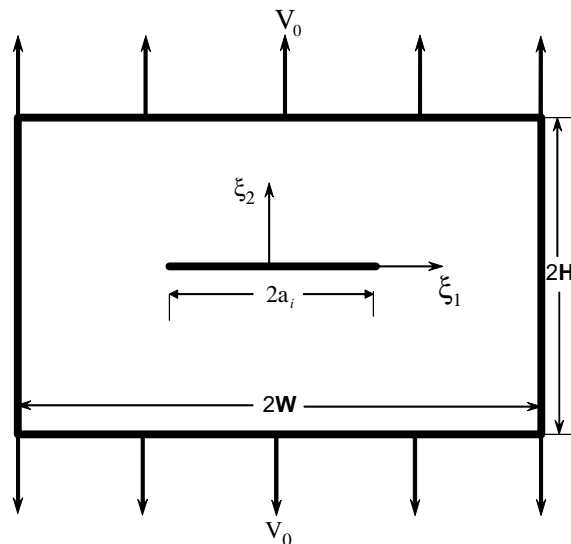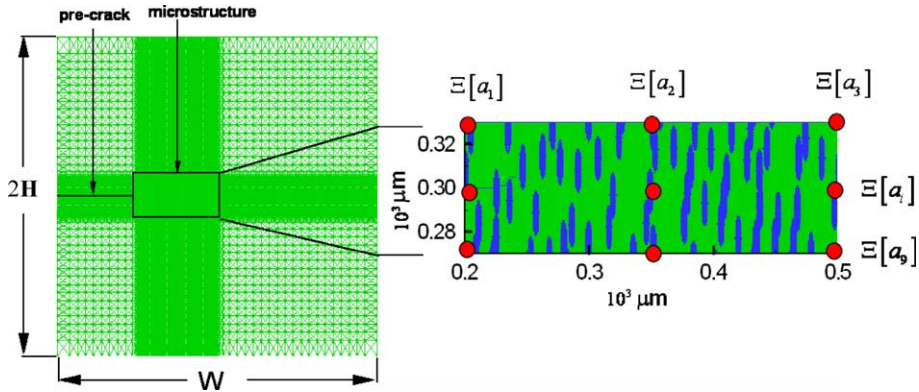

Fig. 2. Specimen configuration for calculations.

Fig. 3. A schematic illustration of the stochastic model.

the top and bottom edges with a linear ramp from zero to this maximum velocity in the first 0.01 μs of loading. All other specimen surfaces have traction-free boundary conditions. Specifically, the loading conditions are

$$\dot{u}_2(\xi^1, \pm H, t) = \begin{cases} \pm \dfrac{t}{0.01} V_0 & t < 0.01 \ \mu s \\ \pm v_0 & t > 0.01 \ \mu s \end{cases} \quad -W < \xi^1 < W \\ T^1(\xi^1, \pm H, t) = 0 \qquad\qquad\qquad -W < \xi^1 < W \\ T^1(\xi^2, \pm W, t) = T^2(\xi^2, \pm W, t) = 0, \qquad -H < \xi^2 < H \end{cases}. \tag{28}$$

This set of conditions represents the loading of the pre-crack by a tensile wave with a stress amplitude of 16.5 MPa $[(\rho C_L)_{material} V_0]$ and a linear ramp from zero to that value in 0.01 μs. The properties of each segment of potential fracture surface are specified according to its location inside the matrix, in the reinforcements or along the matrix/reinforcement interfaces. Xu and Needleman [34] suggested that the maximum strength T_{max} should be between $E/1000$ and $E/200$ with E being the Young's modulus. In this study, $T_{max} = E/700$, $\eta_0 = 0.001$ and $\alpha = 1$ for each constituent and $\Phi_0 = [(1 - v^2)/E] K_{IC}^2$ with K_{IC} being the mode-I fracture toughness of the material in question. The deterministic values of critical separations (Δ_{nc} and Δ_{tc}) are calculated from Eqs. (23) and (24).

During the analysis, the expected value of a material property is taken to be the same as its deterministic value and the stochastic variation is relative to the expected values. Also in this paper, the expected values of materials constants for each phase in a microstructure are spatially homogeneous. A more general treatment with spatially varying expected values of material constants would be interesting since it admits the incorporation of probability functions such as the Weibull or Gaussian distribution in the specification of properties variations. Such an analysis is not pursued here, partly because of the lack of direct experimental data for such a quantification and partly because of an interest in comparing the results here with the results from earlier deterministic analysis of Zhai et al. [16] which was based on an assumption of homogeneous properties in each phase. Under this condition here, the zeroth-order stochastic moment of any dependent quantity (e.g., displacement, a stress component, a strain component, dissipated energy, a cohesive surface traction component, or a component of the cohesive surface separation) corresponds to the deterministic value, allowing integrated deterministic and stochastic analyses to be carried out. The calculations of this paper involve nine nodal points and bilinear shape functions for property interpolation. A detailed description of the framework is provided in Tomar and Zhou [30]. As explained in Eq. (1) of Section 2.1 a
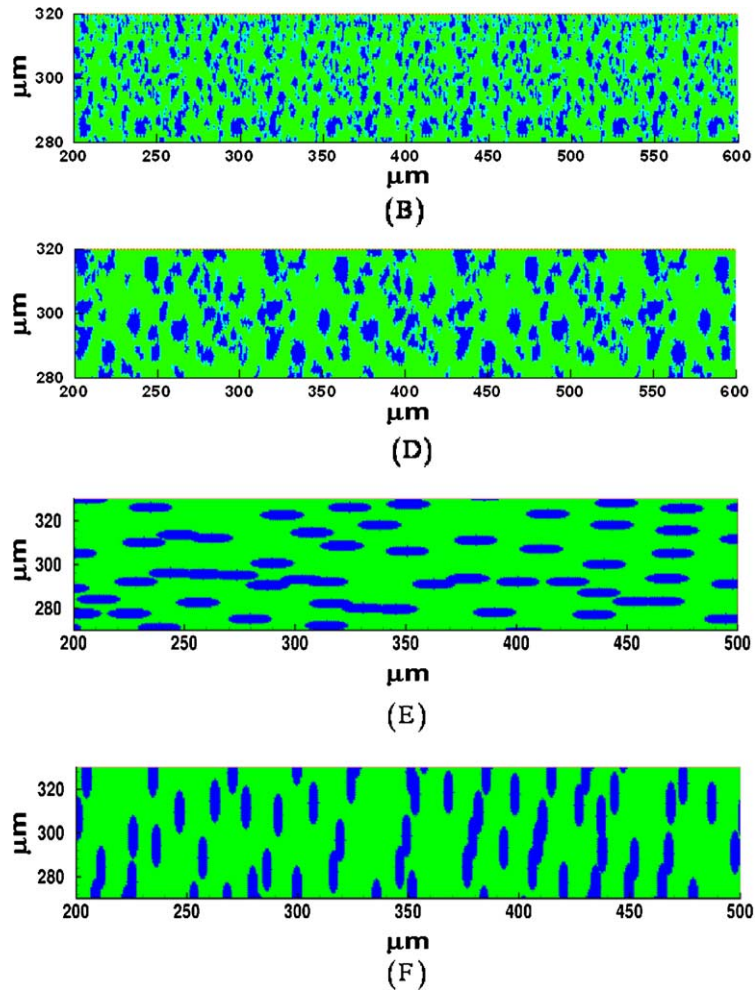
Fig. 4. Microstructures analyzed.

continuous random field is obtained by an interpolation of random property values specified at the inter-polation points. A schematic illustration of the stochastic analyses is shown in Fig. 3.

Fig. 4 shows the microstructures used in the analyses. The labeling of these microstructures follows the convention in Zhai et al. [16] for the ease of direct comparison with the deterministic results. Microstruc-tures B and D are actual phase distributions of materials produced in the laboratory, cf. Logan [25]. These microstructures consist of TiB_2 particles (with average linear intercept length values of approximately 2 μm and 3 μm, respectively) surrounded by an Al_2O_3 phase (with average linear intercept length of approxi-mately 5 μm and 8 μm, respectively). There is a clear difference in the size scales of the phases between the two microstructures. Obviously, analyses using these actual microstructures are useful since they are directly application to actual material samples. On the other hand, the morphological parameters (e.g., grain size, phase volume fraction, and connectivity) for these microstructures are coupled and their effects cannot be analyzed independently. To delineate the influence of different phase attributes, two idealized microstructures (E and F in Fig. 5) are also used in the simulations. The volume fraction of the TiB_2 phase in all four microstructures is 30%. While consisting of the same type of particles, microstructures E and F
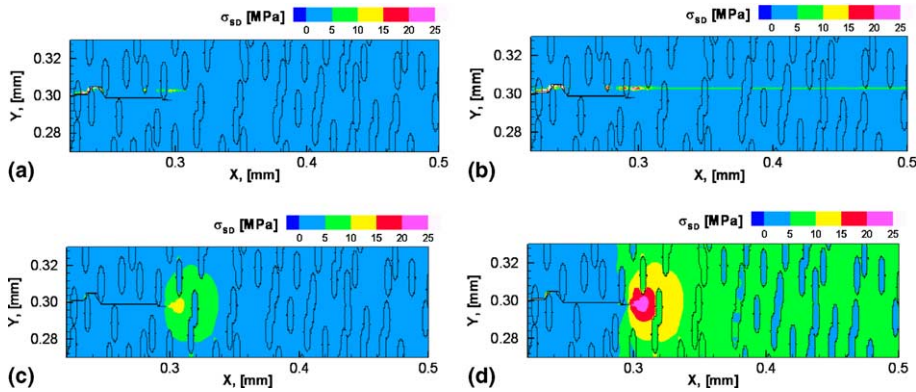
Fig. 5. A comparison of the standard deviations of maximum stress for different combinations of variations in bulk and interfacial properties for microstructure F ($t = 0.12\ \mu$s): (a) case-A; (b) case-B; (c) case-C and (d) case-D.

have two different particle arrangements, representing two orthogonal microstructural orientations. Microstructure E is representative of microstructures in which elliptical particles with the major axis aligned in the direction of the apparent crack path. Microstructure F has a similar phase morphology as microstructure E, except that the minor axis of the elliptical particles is aligned in the direction of the apparent crack path. The randomly distributed unidirectional elliptical particles give rise to orientation-dependent fracture response. The long and short axes of the TiB_2 particles are 10 μm and 2.5 μm, respectively, giving rise to an aspect ratio of 4. For each of these microstructures, only the particular sample as shown is used in the analysis. Multiple microstructural samples are not used here, primarily because of the assumption that the stochastic variations in material properties allow the effects of the fluctuations in local properties on the deformation event to be characterized. This treatment is one of the benefits of the stochastic analysis carried out, in contrast to the approach of using multiple microstructural samples taken in Zhai et al. [16].

The results of second-order perturbation methods converge to the results of direct Monte-Carlo method for properties variations of up to 15% relative to the corresponding mean values, cf. Ghanem and Spanos [26]. Tomar et al. [15] established the conditions for the solution convergence of CFEM models with the mesh sizes and the mean values of the cohesive parameters used. These limits on the model are observed in the analysis carried out here.

To quantify the variation in the fracture behavior of the microstructures, we consider the stress fields and the energy release rate. To delineate the influence of the variations in different independent parameters on the fracture behavior, calculations are first carried out using microstructure F for different combinations of variations in interfacial and bulk properties. Specifically, four cases are analyzed. Case-A ($\beta^{T\max} = 0.05$, $\beta^{A_c} = 0.05$, $\beta^E = 0.0$, and $\beta^v = 0.0$) and case-B ($\beta^{T\max} = 0.10$, $\beta^{A_c} = 0.10$, $\beta^E = 0.0$, and $\beta^v = 0.0$) only involve variations in the interfacial properties. On the other hand, case-C ($\beta^{T\max} = 0.0$, $\beta^{A_c} = 0.0$, and $\beta^E = 0.05$) and $\beta_v = 0.05$) and case-D ($\beta^{T\max} = 0.0$, $\beta^{A_c} = 0.0$, $\beta^E = 0.10$, and $\beta^v = 0.10$) only involve variations in the bulk properties.

Fig. 5 shows the distributions of the standard deviation of the maximum stress for the four cases at time $t = 0.12\ \mu$s. These contour plots show that when there is no stochastic variation in the bulk properties (Fig. 5a and b) the standard deviation of the maximum stress is negligible irrespective of the level of variation in the interfacial properties. However when there is no stochastic variations in the interfacial properties, the average standard deviation of the maximum stress increases from approximately 3% to approximately 6% as the variations in bulk properties change from 5% to 10%. Obviously, variations in stress distribution are primarily due to the stochastic variations in the bulk properties. The corresponding distributions of the

expected value of the maximum stress for these cases (not shown) are nearly the same as those of the maximum stress (not shown) in the fully deterministic case. In fact, the expected value and the deterministic value are essentially the same for all four microstructures analyzed for times up to $t = 0.12$ μs. This finding shows that the second-order stochastic moments have very small or negligible contributions to the expected value compared with the zeroth-order moments. This implies that for the distribution of bulk properties considered here, the level of stochasticity in bulk properties has negligible contribution to the expected value of the stress components.

A comparison of the standard deviations of the maximum stress at $t = 0.12$ μs in the four microstructures in Fig. 4 is given in Fig. 6. The average values are between 5% and 7%. The value for microstructure E is higher over a larger area around crack tip than that in microstructure F. Because microstructure F is believed to offer a significantly higher resistance to crack growth compared with microstructure E, the lower levels of stress variation in microstructure F can be viewed as an indication of smaller range of possible crack length compared with microstructure E. On the other hand, the distributions of the standard deviation of the maximum stress microstructures B and D are quite similar, suggesting similar ranges of fracture behavior variation in these microstructures. More detailed discussions will be given later. The dependence of stress variation on microstructure seen here is consistent with what is discussed in Reusch and Estrin [35]. It appears that microstructures that provide smaller resistance to fracture are associated with larger variations of stress around the mean fields.

Fig. 7 shows the time histories of the expected value of total energy dissipated ϕ, which is defined as $\phi = \int_{S_0} \Phi_d dS$ (see Section 2.3), for all four microstructures. While the difference between the profiles for microstructures B and D is small, the difference between the profiles for microstructures E and F is significant. This indicates that, when all microstructures assume fixed deterministic values of material properties which are equal to their expected values, the difference between the fracture resistances of microstructures B and D is smaller compared with the difference between the fracture resistances of microstructures E and F. Also under such conditions, microstructure F shows the highest resistance to fracture initiation since it has a crack initiation times of approximately 0.09 μs while microstructures B, D, and E have fracture initiation times of approximately 0.07 μs.

To compare the variations of fracture resistances of these microstructures, their time histories of standard deviation of total energy dissipated is plotted in Fig. 8. Three different levels of variation (5%,
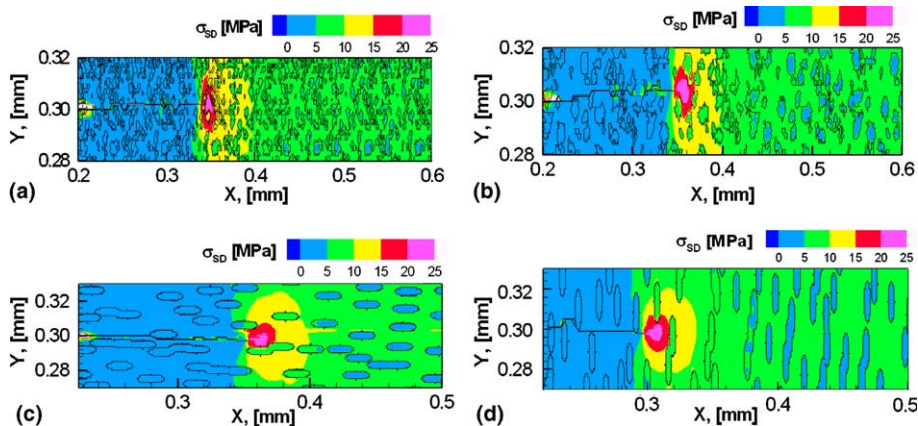

Fig. 6. A comparison of the standard deviations of maximum stress in all microstructures at time $t = 0.12$ μs (10% variation of bulk properties and 0% variation in interfacial properties): (a) microstructure B; (b) microstructure D; (c) microstructure E and (d) microstructure F.
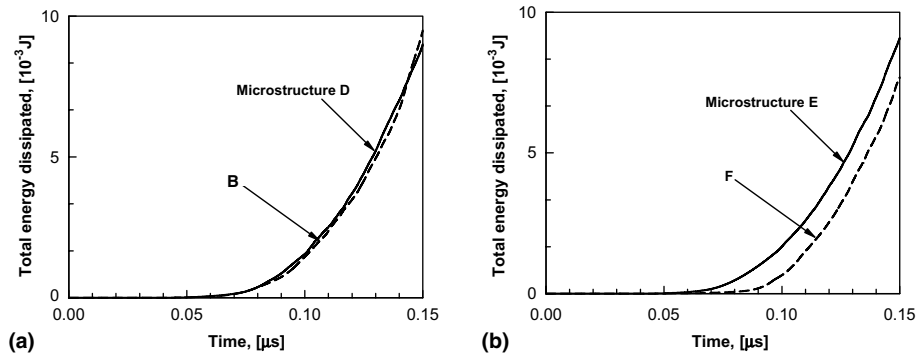
Fig. 7. Time histories of the expected value of total energy dissipated for different microstructures.

10%, 15%) for the interfacial properties (T_{max} and Δ_{nc}) are considered while the variation of the bulk properties (E and v) is held at 0%. The variation in the energy dissipated clearly depends on the microstructures and is highly sensitive to the variation in interfacial properties. In all four microstructures, the average coefficient of variation (the ratio of standard deviation and expected value) which is a measure of the spread of a statistical distribution around the mean value) of the total energy dissipated is approximately 0.005, 0.01, and 0.015 when the variation of the interfacial properties is at 5%, 10%, and 15%, respectively. This trend is weakly dependent on the microstructural morphology involved. Specifically, the range of variation is larger for microstructure E than for microstructure F which has a lower level of expected value of energy dissipated than microstructure E at any give time as seen in Fig. 7. While the lower expected value of the energy dissipated in microstructure F signifies a higher resistance to crack propagation, the higher range of variation of the energy dissipated for microstructure E signifies the possibility of a wider range of variation in fracture outcome in terms of, e.g., crack path and crack length. Such a wider range of variation almost invariably leads to lower fracture resistance in a statistically sense since cracks follow the weakest path. A similar trend of wider range of variation with lower expected value of the energy dissipated is seen for microstructures B and D as well.

To quantify the range of behavior variation, the standard deviation of the total energy dissipated (s_d^ϕ) is used to evaluate an upper limit and a lower limit for the energy release rate. Specifically, the range is $\mu^\phi \pm 3s_d^\phi$. Similarly, the coefficient of variation of the interfacial state variable λ (s_d^λ) is used to obtain a range of variation for crack length which is taken as $\mu^\lambda \pm 6s_d^\lambda$. These choices are relative and correspond to difference confidence levels as discussed in Section 2.3. They are used for relative comparisons between microstructures. Fig. 9 shows the time histories of the range of crack length for microstructures E and F at two different levels of variation (5% and 10%) of interfacial properties. The crack length here corresponds to the total crack surface area generated. Clearly, microstructure has a clear impact on the fracture initiation time. Microstructure E has a higher level of variation of crack length relative to the mean value compared with microstructure F. In both microstructures, the difference between the expected value and the lower limit of the crack length is much larger than the difference between the upper limit and the expected value. This asymmetry in deviations from the mean behavior due to material properties fluctuations suggests that the behavior of the microstructure with the expected values of the materials properties is closer to the behavior in the "worst case scenario" than to the behavior in the "best case scenario" that can be brought about by random fluctuations of material properties. To state it differently, stochastic variations in interfacial behavior in the microstructure provide a much larger potential for enhancing fracture resistance and a smaller opportunity for lowering the fracture resistance, as measured in terms of crack length. The reason for this is that cracks always tend to follow the weakest path in a microstructure. Under the
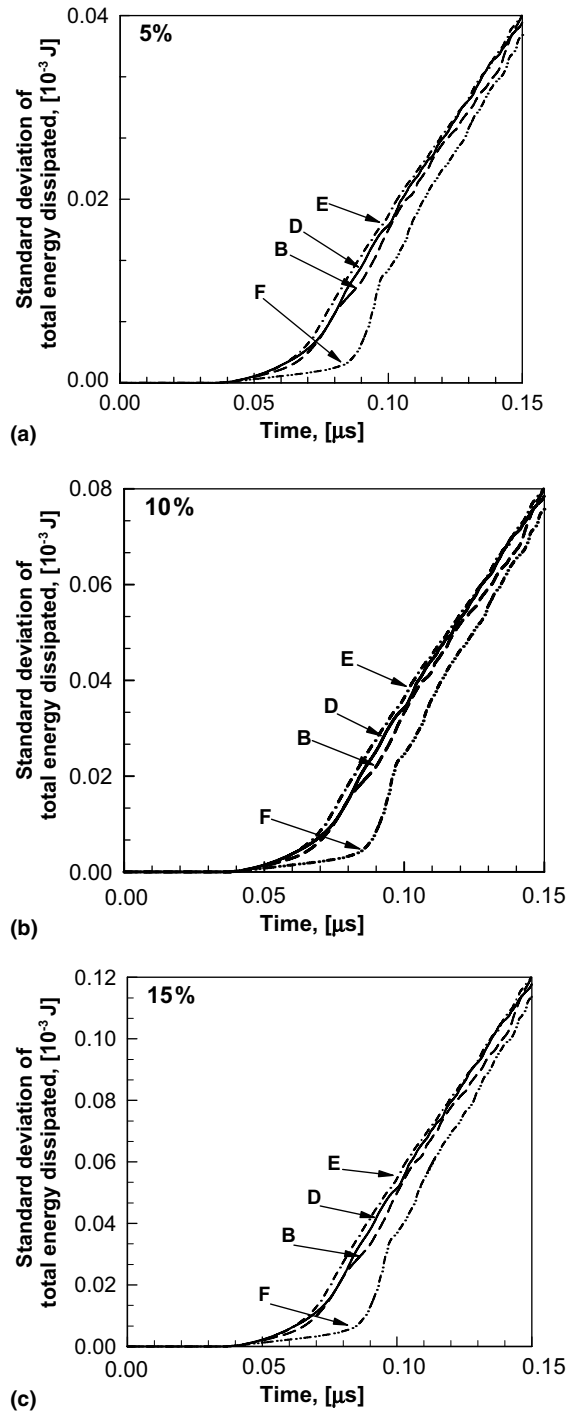
Fig. 8. Time histories of the standard deviation of total energy dissipated for different microstructures at different levels of variations of interfacial properties, the variation of the bulk properties is held at 0%.
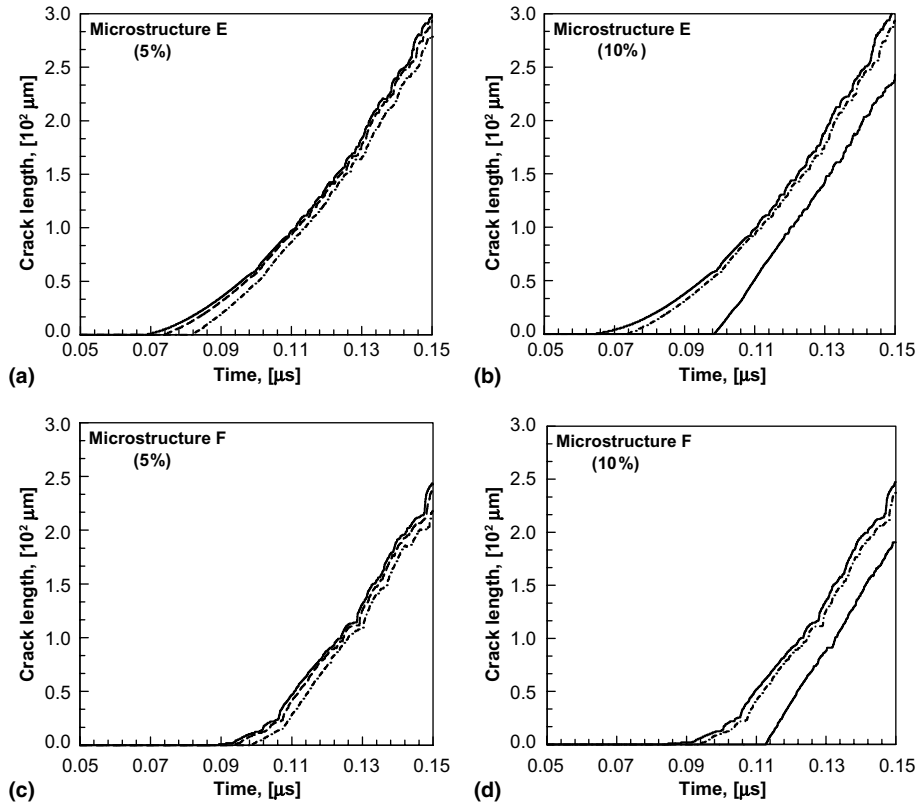
Fig. 9. Time histories of the range of crack length in microstructures E and F at different levels of property variations (the three curves give the upper limit, the expected value and the lower limit of crack length, respectively).

conditions of a uniform distribution of material properties at the expectation values, the weakest path is quite similar to those in microstructures with properties which are random variations from the expected values. Since cracks always follow the weakest path, the difference between the "expected scenario" and the "best case scenario" is certainly larger than that between the "expected scenario" and the "worst case scenario". Geometrically, it is possible to find crack paths that would pose much higher resistances to fracture by randomly varying local properties. Although randomness "can potentially" lead to increase in fracture resistance, such higher resistance paths may not be followed. For microstructure E, the average deviation of crack length to the lower side is approximately 6% of the expected value for a 5% variation of interfacial properties and approximately 20% of the expected value for a 10% variation of interfacial properties. For microstructure F, the average deviation to the lower side is approximately 8% of the expected value for a 5% variation of the interfacial properties and approximately 25% of the expected value for a 10% variation of the interfacial properties. The deviation to the upper side is much less, at approximately 2% to 5% of the expected value for variations of interfacial properties between 5% and 10% for microstructure E. For microstructure F, the deviation to the upper side is approximately 3% to 6% of the expected value for the same amount of variation in properties.

It is noted that the deviation of crack length to the lower side increases rapidly as the variation in interfacial properties is raised beyond 15%. An analysis in that range is not carried out since those conditions can not be accurately characterized by the second-order perturbation pursued here.
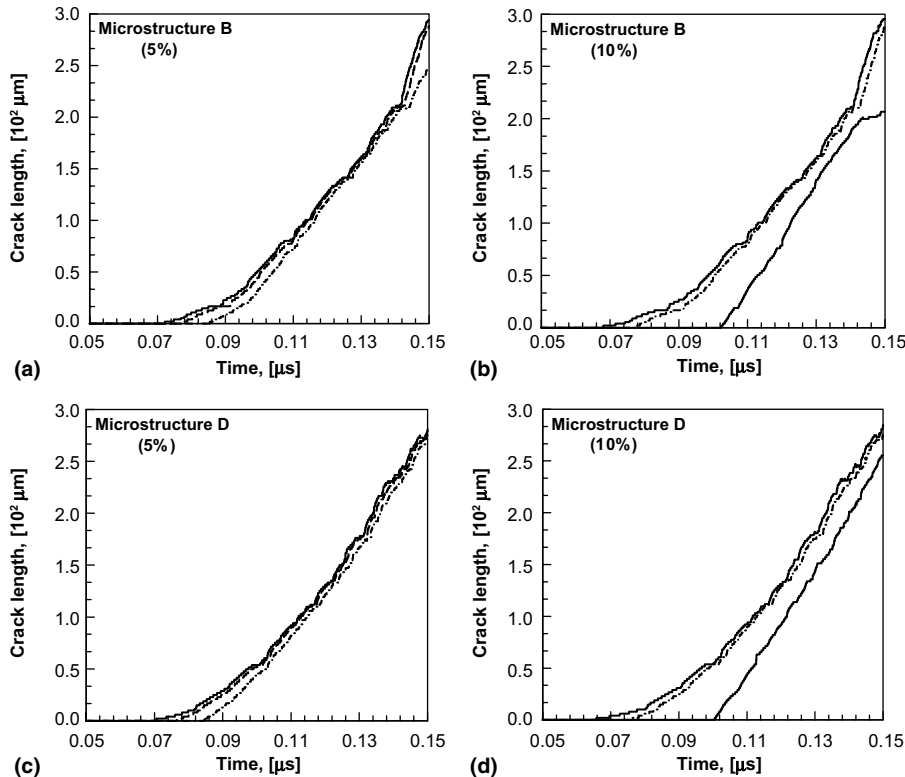
Fig. 10. Time histories of the range of crack length in microstructures B and D at different levels of property variations (the three curves give the upper limit, the expected value and the lower limit of crack length, respectively).

As shown in Fig. 10, the expected value of the total crack length and its variation for microstructures B and D follow a similar trend as seen in Fig. 9 for microstructures E and F. At any instant of time, the crack length for microstructure D is smaller than that for microstructure B. This is because of the difference in the morphological construction of these two microstructures. The average variation in the lower limit of crack length is approximately 6% of the expected value at a 5% level of variation in interfacial properties and approximately 15% of the expected value at a 10% level of variation in interfacial properties in microstructure B. For microstructure D, the average variation in the lower limit of crack length is approximately 4% of the expected value at a 5% level of variation in interfacial properties and approximately 12% of the expected value at a 10% level of variation of interfacial properties. The upper level is less sensitive to the level of variation of interfacial properties. It changes by approximately 2–3% of the expected value when the variation of interfacial properties changes from 5% to 10% in microstructure B. For microstructure D, it changes by approximately 2–4% of the expected value over the same range of change in properties variations. We also note that microstructures showing wider range of variation of crack growth have higher variations of crack initiation time (Figs. 9 and 10).

The variation of energy release rate as a function of property variations is important in the characterization of fracture resistance. Fig. 11 shows the range of energy release rate for the four microstructures over the time period of up to $t = 0.15$ μs. Significant variations are observed for all microstructures with the increase in the level of variation of interfacial properties. Specifically for microstructures E and F, approximately 3% to 6% variations relative to their expected values are seen for variations of interfacial
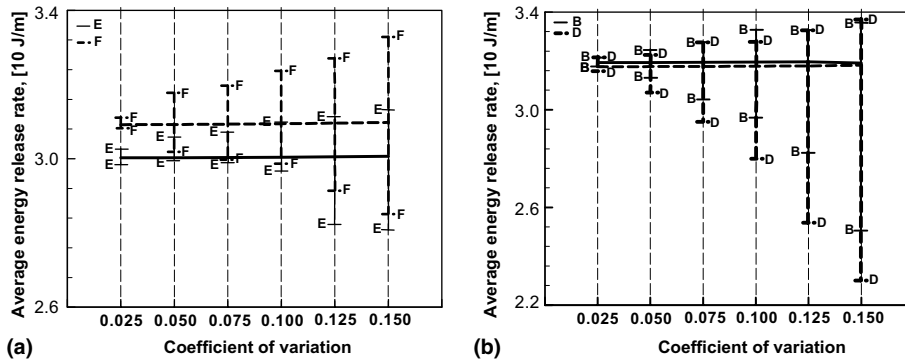
Fig. 11. A comparison of the average energy release rate for: (a) microstructures E and F and (b) microstructures B and D at different values of coefficient of variation for interfacial properties while the bulk properties are fixed at their expected values (time $t = 0.15$ s).

properties between 5% and 10%. For microstructures B and D, approximately 2.5–4% variations relative to their expected values are seen for variations of interfacial properties between 5% and 10%. In addition, the range of energy release rate is wider for microstructure F than for microstructure E. Similarly, the range of energy release rate is wider for microstructure D than for microstructure B. The larger particle size in microstructure D relative to that in microstructure B appears to give rise to the higher level of variation in the energy release rate. For all microstructures, the difference between the upper limit and the expected value of the average energy release rate is higher than the difference between the expected value and the lower limit of the average energy release rate. This again indicates that an increase in the random variation of properties has an asymmetric effect on the variation of the energy release rate. Note that the analysis here
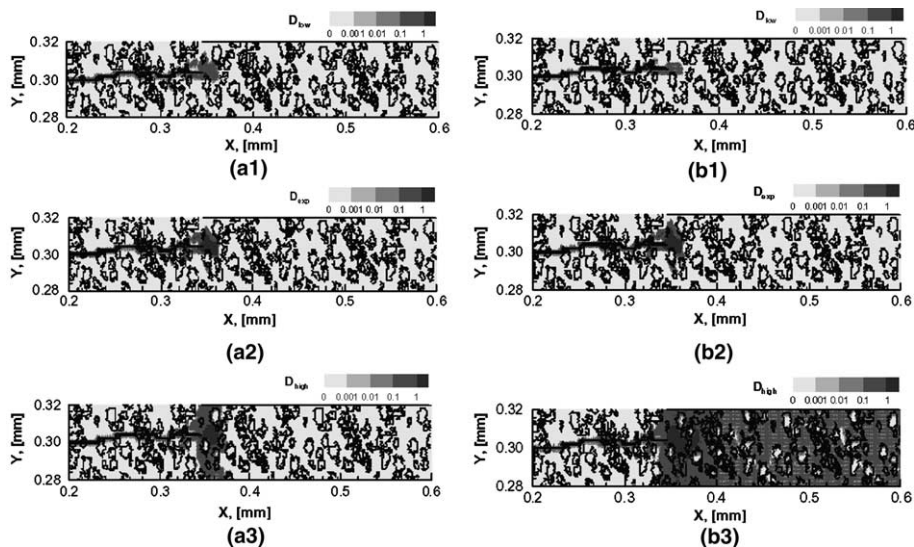

Fig. 12. Contours of the damage parameter in microstructure D at different levels of variation of interfacial properties while the bulk properties are fixed at their expected values (time $t = 0.12$ μs), (a1, a2, and a3) 5% variation properties, (b1, b2, and b3) 15% variation of properties.

concerns only the range of variation and does not address the issue of probability distribution of events. This result only suggests that, with random variations of properties, the difference between the maximum value and the expected value of the energy release rate is larger than the difference between the expected value and the minimum value.

To quantify the variation of the damage parameter D with the random variation of material properties, its range is calculated for different levels of variations in interfacial properties. First, we note that the range of variation for D depends only on $\beta^{\Delta_{nc}}$. Calculations show that the expected value of D is essentially the same as its deterministic value (not shown) throughout the microstructure. Fig. 12 shows the range of the damage parameter D for microstructure D at $t = 0.12$ μs for two different levels of variation of interfacial properties. Clearly, the variation in interfacial properties offers more opportunities (spatially) for cracks to nucleate, resulting in more diffused distribution of damage. The wider distribution of damage into cracks that do not lead to full separation or total failure provides a mechanism for energy dissipation, thus reducing the driving force for the propagation of major cracks that lead to full separation. Overall, the results show that a propagating crack is most likely to propagate along the path which offers the lowest resistance. In all microstructures the difference between the higher end of the damage range and the expected level of the damage range is higher and more sensitive to the variation of the interfacial properties than the difference between the expected level of damage and the lower end of the damage range. This result indicates a bias in the effect of the randomness of the material properties on the damage range.

4. Conclusion and remarks

A framework for combined deterministic and stochastic analyses of dynamic fracture in heterogeneous microstructures is presented. This framework has been used to analyze fracture processes in idealized and real microstructures of a two-phase Al_2O_3/TiB_2 ceramic composite system. The effect of random variations in material properties of up to 15% from their mean values is analyzed with an explicit account of random crack development. Calculations focus on analyzing the fracture response variation with varying levels of variation of material properties for a particular microstructural morphology as well as on analyzing the variations in fracture response with variations in microstructural morphology. The analyses of hypothetical phase morphologies focused on the effect of phase morphology. The analyses on real microstructures established the correlation between the inherent randomness in material properties and range of fracture response. In all microstructures, the behavior for microstructures with the expected values of the constituent properties are essentially the same as the deterministic behavior and are the same as those in Zhai et al. [16].

Calculations show that the lower bound for the fracture response is very close to the response of a material whose phases possess the expectation values of the randomly varying material properties. In addition, the effect of property variations on the variation of crack length, energy dissipation, and damage is asymmetric with a strong bias towards "worst case scenario". This indicates that improper account of material property randomness or, in some cases assumption of deterministic material property, might reflect material performance that is stronger than actual. This conclusion is intricately linked to underlying microstructural morphology. A microstructure less prone to fracture shows higher variations in fracture response when compared to the one which offers least resistance to the crack propagation. The range of total crack length and the range of average energy release rate are found to be dependent upon microstructure as well as properties variations. For a particular microstructural morphology, the levels of variations in the crack surface area generated and the variations in the energy release rate are of the same order as the levels of variations in constituent properties. The observations support the conclusion that a material designer needs to make conservative estimates for a material's performance if its microstructural construction imparts uncertainty to local material properties.

Acknowledgement

References

[1] Alzebdeh K, Ostoja-Starzewski M. Micromechanically based stochastic finite elements. Finite Elem Anal Des 1993;15:35–41.
[2] Alzebdeh K, Ostoja-Starzewski M. Micromechanically based stochastic finite elements: length scales and anisotropy. Prob Engng Mech 1996;11(4):205–14.
[3] Weibull W. The phenomenon of rupture in solids. Proc R Swed Inst Engng Res (Ing Akad Handl) 1939;153:1–55.
[4] Weibull W. A statistical distribution function of wide applicability. ASME J Appl Mech 1951;18(3):293–7.
[5] Batdorf SB. Fundamentals of the statistical theory of fracture. Fract Mech Ceram 1978;3:1–30.
[6] Duxbury PM, Kim SG, Leath PL. Size effect and statistics of fracture in random materials. Mat Sci Engng 1994;176:25–31.
[7] Dai H, Frantziskonis G. Heterogeneity, spatial correlations, size effects and dissipated energy in brittle materials. Mech Mater 1994;18:103–18.
[8] Zhou F, Molinari J-F. Stochastic fracture of ceramics under dynamic tensile loading. Int J Solids Struct 2004;41:6573–96.
[9] Xu XP, Needleman A. Void nucleation by inclusion debonding in a crystal matrix. Mod Simulat Mater Sci Engng 1993;1(2):111–32.
[10] Miller O, Freund LB, Needleman A. Energy dissipation in dynamic fracture of brittle materials. Mod Simulat Mater Sci Engng 1999;7:573–86.
[11] Miller O, Freund LB, Needleman A. Modeling and simulation of dynamic fragmentation in brittle materials. Int J Fract 1999;96(2):101–25.
[12] Xuan W, Curtin WA, Needleman A. Stochastic microcrack nucleation in lamellar solids. Engng Fract Mech 2003;70:1869–84.
[13] Zavattieri PD, Raghuram PV, Espinosa HD. A computational model of ceramic microstructures subjected to multi-axial dynamic loading. J Mech Phys Solids 2001;49:27–68.
[14] Zavattieri PD, Espinosa HD. Grain level analysis of crack initiation and propagation in brittle materials. Acta Mater 2001;49:4291–311.
[15] Tomar V, Zhai J, Zhou M. Bounds for element size in a variable stiffness cohesive finite element model. Int J Numer Methods Engng 2004;61:1894–920.
[16] Zhai J, Tomar V, Zhou M. Micromechanical modeling of dynamic fracture using the cohesive finite element method. J Engng Mater Tech 2004;126:179–91.
[17] Liu WK, Belytschko T, Mani A. Random field finite elements. Int J Numer Methods Engng 1986;23:1831–45.
[18] Baecher GB, Ingra TS. Stochastic FEM in settlement predictions. J Geotech Engng Div 1981;107(GT4):449–63.
[19] Vanmarcke E, Grigoriu M. Stochastic finite element of simple beams. J Engng Mech 1983;109(5):1203–14.
[20] Lawrence MA. Basis random variables in finite element analysis. Int J Numer Meth Engng 1987;24:1849–63.
[21] Liu WK, Besterfield G, Belytschko T. Transient probabilistic systems. Comp Methods Appl Mech Engng 1988;67:27–54.
[22] Araujo JM, Awruch AM. On stochastic finite elements for structural analysis. Comput Struct 1993;52(3):461–9.
[23] Liu WK, Belytschko T, Lua YJ. Probabilistic finite element method. In: Sundararajan C, editor. Probabilistic structural mechanics handbook: theory and industrial applications. p. 70–105.
[24] Zhao JP, Huang WL, Dai SH. The application of 2D elastic stochastic finite element method in the field of fracture mechanics. Int J Pres Ves Piping 1997;71:169–73.
[25] Logan KV. Composite ceramics, final technical report, USSTACOM DAAEO7-95-C-R040; 1996.
[26] Ghanem RG, Spanos PD. Stochastic finite elements: a spectral approach. New York: Springer-Verlag; 1991.
[27] Shet C, Chandra N. Analysis of energy balance when using cohesive zone models to simulate fracture processes. J Engng Mater Tech 2002;124:440–50.
[28] Krieg RD, Key SW. Transient shell response by numerical integration. Int J Numer Methods Engng 1973;7:273–86.
[29] Belytschko T, Chiapetta RL, Bartel HD. Efficient large scale non-linear transient analysis by finite elements. Int J Numer Methods Engng 1976;10:579–96.
[30] Tomar V, Zhou M. Deterministic and stochastic analyses of dynamic fracture in two-phase ceramic microstructures with random material properties [manuscript in preparation].
[31] Minnaar, K. Experimental and numerical analysis of damage in laminate composites under low velocity impact loading. PhD Thesis, Georgia Institute of Technology; 2002.

[32] Lin YK. Probabilistic theory of structural dynamics. New York: McGraw-Hill; 1967.
[33] Nigam NC. Introduction to random vibrations. Cambridge, MA: The MIT Press; 1983.
[34] Xu XP, Needleman A. Numerical simulations of fast crack growth in brittle solids. J Mech Phys Solids 1994;42:1397–434.
[35] Reusch F, Estrin Y. FE-analysis of mechanical response of simple structures with random non-uniformity of material properties. Comput Mater Sci 1998;11:294–308.